IEEE Access
Multidisciplinary | Rapid Review | Open Access Journal

Received 21 March 2023, accepted 13 April 2023, date of publication 19 April 2023, date of current version 26 April 2023.

Digital Object Identifier 10.1109/ACCESS.2023.3268520

RESEARCH ARTICLE

Development of Seismic Intensity Maps Using Low-Cost Micro-Electro-Mechanical Systems Seismic Network

JAE-KWANG AHN[1], JANGSOO LEE[2], YOUNG-WOO KWON[2], (Member, IEEE), JUNG-KYU KIM[3], AND DONG YOUP KWAK[4]

[1]Earthquake and Volcano Technology Team, Korea Meteorological Administration, Seoul 07062, South Korea
[2]Department of IT Engineering Computer Science, Kyungpook National University, Daegu 41566, South Korea
[3]Infra BM, SK Telecom, Seoul 04539, South Korea
[4]Department of Civil and Environmental Engineering, Hanyang University, ERICA Campus, Ansan, Gyeonggi-do 15588, South Korea

Corresponding author: Dong Youp Kwak (dkwak@hanyang.ac.kr)

This work was supported by in part by the Korea Meteorological Administration under Grant KMA2022-02121, and in part by Hanyang University under Grant HY-2019-N.

ABSTRACT The low-cost IoT seismometer (LCIS), which embeds a micro-electro-mechanical systems accelerometer and LTE communication sensor, has been developed and deployed in South Korea. Currently, approximately 7,000 stations (with an average density of 0.07/km^2) with LCIS devices are operating in real-time, which is about 25 times higher density than the national seismic network with high performance seismometers. This study shows a method for processing LCIS data and plotting an intensity map considering its installation characteristics and density. The majority of LCISs are installed inside buildings, so an adjustment converting to the free-surface equivalent vibration is applied. Seismic intensity maps are derived using only high-density LCIS network data, which showed very similar distributions to the maps from the high-performance seismometer network. This validates the usefulness of the LCIS, a low-cost but new technology on seismic network devices, for the generation of high-resolution seismic intensity map and earthquake early warning systems.

INDEX TERMS MEMS, modified mercalli intensity (MMI) map, high density seismic network, South Korea seismic network, ground motion model.

I. INTRODUCTION

Earthquake early warning (EEW) technologies include rapid detection and public alert systems that aim to warn against possible significant damages (i.e. human casualties as falling) following an earthquake [1], [2]. One widely used approach is network-based EEW, which estimates hypocenter information by analyzing P waves from at least three seismic observatories [3], [4], [5]. Once an earthquake occurs, the closest three observatories would detect the seismic signals first, then EEW system is activated. Hence, EEW performance depends on the density of the observation network because the faster the P wave is observed at least three observatories, the more rapid and efficient the EEW system is achieved [6].

The denser seismic network also helps to create more accurate intensity maps by earthquake events. It is essential to determine the seismic intensity at either damaged locations or undamaged locations for immediate countermeasures (e.g., locating administrative forces on damage-prone regions) and seismic design studies (e.g., study of damage severity of structure based on intensity measures). Note that the Modified Mercalli intensity scale (MMI) is used as the seismic intensity evaluation in South Korea. The MMI map can provide the severity of ground shaking at desired locations. However, expanding seismic observatories is limited for several reasons. First, it is difficult to identify locations with low-level background noise. Second, installation and maintenance costs of real-time observatories with high-performance seismometers are high. Finally, for some locations, it is challenging to establish an observatory

The associate editor coordinating the review of this manuscript and approving it for publication was Qilian Liang.

due to access restrictions such as privately-owned land. These reasons could impede the establishment of dense networks.

Micro-Electro-Mechanical Systems (MEMS) technology, developing based on micromachining and advancements in silicon processing, has been tremendously successful in physical sensing applications [7]. MEMS offer many benefits, including high sensitivity, fast response, low power consumption, and small form factor, which have made them popular in various fields [8]. The MEMS acceleration sensor can record ground shaking efficiently which was confirmed from the shake table tests [9], [10], [11], [12]. In particular, MEMS devices are advantageous in that they can be attached to various types of equipment [13], [14].

MEMS sensors are used in EEW as auxiliary seismic networks around the world. In the United States, the Quake-Catcher Network (QCN) and Community Seismic Network (CSN) projects use standalone MEMS accelerometers and the MyShake project uses the MEMS accelerometer in the smartphone to detect earthquakes [15], [16]. The limitation of QCN and CSN is that they need to connect MEMS accelerometers with other network-capable devices (e.g., laptop or desktop) [17]. The MyShake project uses smartphones allowing anonymous users to record acceleration data and function as potential seismometers. The MyShake was reported to perform similarly to a real-time based-EEW system [17]; however, it requires users to install the application and run it continuously which drains the battery. In regions where earthquakes are infrequent, there are few MyShake users with continuous running. Another example of using MEMS for earthquake warning is the Taiwanese P-alert, which is a MEMS-type accelerometer for EEW applications that are distributed and in operation [18]. P-alert can successfully generate alerts based on real-time signals processed at the field site [19], and can be used individually or as part of the national EEW network [20]. EEW systems utilizing P-alert instruments are more efficient than conventional systems because of their low cost. The limitation of the P-alert is that it requires a computer to process the data at each point. In China, researchers are currently developing and testing an integrated technology of EEW based on MEMS sensors [21], [22].

Korea Meteorological Administration (KMA) in collaboration with SK Telecom (SKT) and Kyungpook National University developed the next-generation EEW system, which combines MEMS and national cellular network [23]. We developed a device detecting seismic motion through the MEMS accelerometer and telecommunicating the real-time data through the LTE Cat.M1 cellular network. This pilot technology is the part of our broader effort to expand the use of IoT devices, and we called it the low-cost IoT seismometer (LCIS).

LCIS-based network system has some notable new features from other MEMS instruments; 1) it uses an LTE wireless communication network and does not require a separate GPS sensor, 2) the system, called ''CrowdQuake,'' has been newly established to process the large amount of real-time data [24], and 3) it is scalable thanks to implementing SKT's infrastructure resources.

CrowdQuake uses approximately 7,000 LCIS devices and a deep-learning-based earthquake signal detection algorithm. Currently, the beta version of CrowdQuake has been in operation over two years and, at the time of writing, has detected 41 small- and medium-magnitude earthquakes. From several earthquake detections, we found that the LCIS records were in accordance with the records of the existed national KMA network. Therefore, in this study, we developed a method to draw an MMI map using sole LCIS data. Previously we verified the reliability of sensors used in CrowdQuake by comparing seismograms from the devices used in the national network [20].

P-alert effectively generates intensity measure (IM) maps [26]; however, P-alert is based on the ShakeMap [25] and uses MEMS measurement data without considering environmental factors (e.g., installation location and ambient noise). In a previous study [27], we showed that the MMI of MEMS is affected by the installation environments such as location or position. This study shows a data processing method eliminating environmental effects and the generation of an MMI map based on MEMS data without ShakeMap.

II. LCIS CERTIFICATION TEST AND INSTALLATION

We ensured the performance of the LCIS through certification tests. Table 1 summarizes the Korean standard for the accelerometer certification test, which outlines the required ranges for sensitivity, frequency response, and linearity [28].

TABLE 1. Accelerometer criteria set from the KMA.

	Sensitivity	Frequency response	Linearity
Frequency	1 Hz	1, 2, 4, 8, 16, 20 Hz	8 Hz
Amplitude	H: 1 m/s^2 V: 0.4 m/s^2	H: 1 m/s^2 V: 4 m/s^2	10% less: 1 point 90% over: 1 point 10%–90%: 3 points
Allowable error	1% less	3% less	Error: 1% less

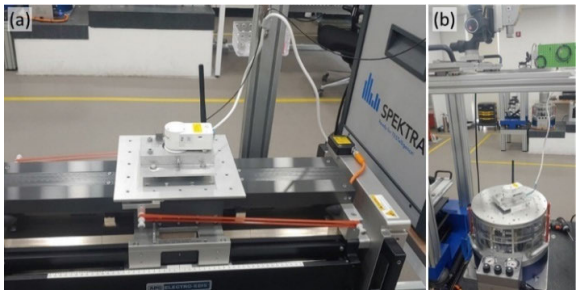

FIGURE 1. Snapshot of certification tests: (a) horizontal direction, (b) vertical direction.

The LCIS can record acceleration in triaxial directions, at a set range of ±2.5g. We tested dynamic responses of

three LCIS devices for each direction and checked them against the standard (Fig. 1). The results are summarized in Table 2. The LCIS accelerometer satisfies requirements of sensitivity, frequency response, and linearity. However, it is not suitable for precise seismic observations because of its low dynamic response level (−72 to −75 dB). The high-performance accelerometer used in the KMA seismic network has dynamic response level of −100 dB or less.

The LCIS offers two major advantages: 1) it can be connected anywhere with an outlet and 2) there is no need for a separate wire connection. We installed the LCISs in various places, and representative cases are shown in Fig. 2. Some devices were installed on the floor of seismic observatories to compare the records with the KMA seismometer (Fig. 2a). In most cases, the devices were installed on the wall outlet of buildings (Fig. 2b). However, installing the LCIS on building walls also means that it records not only seismic waves but also building responses and artificial vibrations, which can affect its performance. In particular, we observed high noise levels when the device was installed in a steel box on a utility pole (Fig. 2c) or temporary wall (Fig. 2d).

FIGURE 2. Examples of low-cost IoT seismometer (LCIS) installation locations: (a) building floor, (b) wall outlet, (c) utility pole, (d) temporary wall.

Due to the installation condition and the surrounding environment, the LCIS has wide range of noise levels. Fig. 3 shows levels of response spectrum for local earthquakes with magnitude 2.5, 3.5, and 7 with source-to-site distance of 10 km (brown lines, based on Clinton and Heaton [29]), high-noise ambient vibration (red line, proposed by Peterson [30]), and dynamic response with noise of LCISs in operation (black lines) and its median level (blue line). The range of LCIS noise levels is from −70 to −10 dB, with average of −63 dB. With this average noise level, vibrations lower than intensity grade of II cannot be detected. Note that to detect an earthquake signal, the noise level of seismometers should be lower than the response spectrum of the seismograms. Considering the proposed noise level from the empirical analysis by Cauzzi and Clinton [31], the LCIS can detect the earthquake signal with a magnitude of 3.5 within 10 km

TABLE 2. Results of KMA certification test of the LCIS.

Direction	Item	1	2	3
X	Sensitivity	0.0%	0.0%	0.1%
	Frequency response	0.5%	0.9%	0.7%
	Linearity	< 0.2%	< 0.4%	< 0.2%
	Dynamic response	−75.2 dB	−75.6 dB	−71.2 dB
Y	Sensitivity	0.1%	0.0%	0.0%
	Frequency response	1.5%	1.4%	0.8%
	Linearity	< 0.1%	< 0.3%	< 0.2%
	Dynamic response	−74.1 dB	−73.0 dB	−67.5 dB
Z	Sensitivity	0.0%	0.2%	0.0%
	Frequency response	0.8%	0.7%	0.8%
	Linearity	< 0.3%	< 0.2%	< 0.7%
	Dynamic response	−74.5 dB	−72.3 dB	−73.6 dB

distance in average. In the case of low-noise LCIS, it can detect the signal with a magnitude of 2.5, but in the case of high-noise LCIS, only signals with magnitude greater than 3.5 within 10 km distance can be detected.

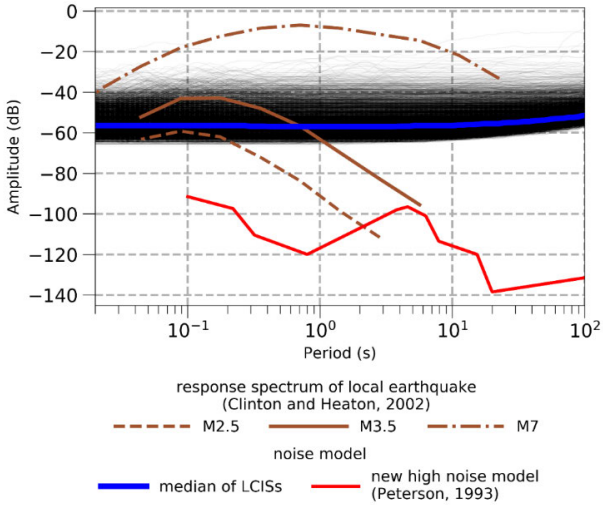

FIGURE 3. Noise characteristics for low-cost IoT seismometer (LCIS; black) responses to earthquake data at 10 km (brown lines). Blue and red lines show the median and high-noise models.

III. PRE-PROCESSING OF LCIS SEISMIC DATA

More than 7,000 LCISs have been installed in various locations in South Korea and are currently in operation. Rather than strictly control the installation following suggested conditions (i.e., on the 1st floor in low-rise building), LCISs have been spread out and installed if security and maintenance can be kept. The post office, fire station, and cellular network station are majority of host buildings. From these installation conditions, we identified three primary issues. The first is that the position of the triaxial sensor is not orthogonal to the gravity, and the second is that the background noise impairs sensor readings. Third, the building response alters the amplitude of motions.

To resolve the first issue, we applied the rotation transformation matrix to accelerometer vectors [32], [33].

Since the MEMS accelerometer in LCIS can detect the gravity, the rotation angle (θ) required to set the sensor position orthogonal to the gravity direction can be calculated at static condition. Once θ is calculated, we can compute the transformation matrices that map the signals in horizontal and vertical directions as follows [34]:

$$R_x(\theta) = \begin{bmatrix} 1 & 0 & 0 \\ 0 & cos(\theta) & -sin(\theta) \\ 0 & sin(\theta) & cos(\theta) \end{bmatrix} \quad (1)$$

$$R_y(\theta) = \begin{bmatrix} cos(\theta) & 0 & sin(\theta) \\ 0 & 1 & 0 \\ -sin(\theta) & 0 & cos(\theta) \end{bmatrix} \quad (2)$$

$$R_z(\theta) = \begin{bmatrix} cos(\theta) & sin(\theta) & 0 \\ sin(\theta) & cos(\theta) & 0 \\ 0 & 0 & 1 \end{bmatrix} \quad (3)$$

where $R_x(\theta)$, $R_y(\theta)$, $R_z(\theta)$ denote transformation matrix for two horizontal directions (x and y) and a vertical direction (z). By rotating the axes as amount of θ, the new acceleration vector can be calculated as follows:

$$\begin{bmatrix} a'_x \\ a'_y \\ a'_z \end{bmatrix} = R_z(\theta)R_y(\theta)R_x(\theta) \begin{bmatrix} a_x \\ a_y \\ a_z \end{bmatrix} \quad (4)$$

where a_x, a_y, and a_z are original acceleration vectors, a'_x and a'_y are horizontal acceleration vectors, and a'_z is the vertical acceleration vector. Following this process, we can estimate horizontal accelerations regardless of sensor installation position.

The second issue is the high background noise. The LCIS data includes building shaking, the device's self-noise, and environmental noise near the sensor. Since the LCIS has a high level of self-noise (Fig. 3), the noise vibration boosts the signal so that we obtain IMs higher than those of the high-performance sensor from the national seismic network even though two sensors are collocated. Therefore, the impact of noise on data needs to be minimized before an MMI map is computed. We propose to do it with appropriate bandpass filters. The range of the bandpass filter is decided by comparing Fourier amplitude spectrum of noise windows and signal windows [35], [36]. This method is widely used when performing signal processing on seismic motions [37], [38], [39].

The third issue is the building response. Since the LCIS is installed inside a building, the recorded motion includes the building response as well as the free-surface ground motion. The building response can amplify or de-amplify the acceleration of the LCIS, depending on the natural frequency of the building and the frequency content of the ground motion. Multi-degree of freedom (MDOF) analysis can be used to eliminate this response. MDOF analysis models a building to a multi-degree of freedom structure, calculates the structure's response to a ground motion, and from the result, the response for a particular floor can be estimated. Therefore, we could understand the response of a multi-floor building to ground motion, then transform the amplitude of the LCIS into the free-surface equivalent amplitude by applying the inverse of the amplification ratio [40].

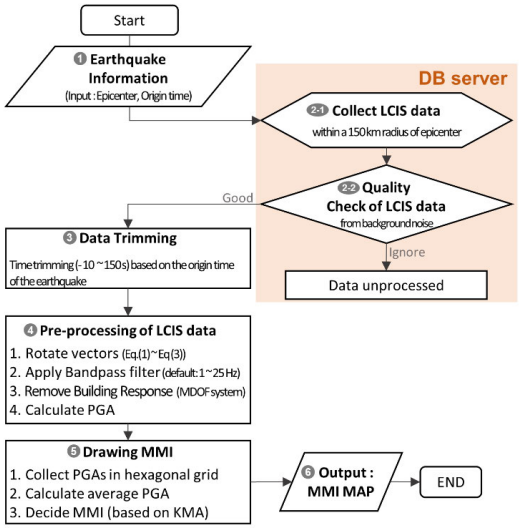

FIGURE 4. Procedure diagram of Crowdquake-intensity-map.

Our solution to calculate the IM for removing the building response and for correcting the sensing directions are available at the GitHub website (https://github.com/knusslab/crowdquake-intensity-map). This algorithm is called Crowdquake-Intensity-Map (CIM) and follows a specific data processing sequence; 1) a user inputs the epicenter and origin time of the earthquake information; 2) a DB server provides the LCIS records by collecting LCIS data within a 150 km radius around the epicenter and checking the quality of the LCIS data (i.e., disregard bad signals checking the noise level of the pre-event records with 1 hour duration ahead the event); 3) the data is trimmed with -10 to 150 seconds from the origin time; 4) horizontal component records are processed using the processing method presented in Section III; 5) the average intensity is decided in a hexagonal grid presented in Section IV; 6) as the final step, the MMI map is output. This data processing sequence creates accurate and reliable intensity map. In addition to an intensity map, earthquake records are provided on the web after being converted into data [41]. These data are provided in two forms for user convenience—MiniSEED [42] and CSV—to use in analyses, for example, PostreSQL [43], site response computation [44], data science, and so on.

Fig. 5 illustrates the change of LCIS acceleration through the conversion process. The seismic record is from an earthquake with M_L 4.9 that occurred on 14 December, 2021, and recorded at the GOS2 and SGP seismic observatories on Jeju island (Fig. 5a). In the GOS2, a high-performance seismometer was on the ground surface with collocated LCIS. The original LCIS data showed that the baselines were not zero for the X and Z directions and not the gravity for the Y direction, even though the position was the same as the seismometer (Fig. 5b). We found the directions of the gravity and the north pole and rotated axes to have two horizontal

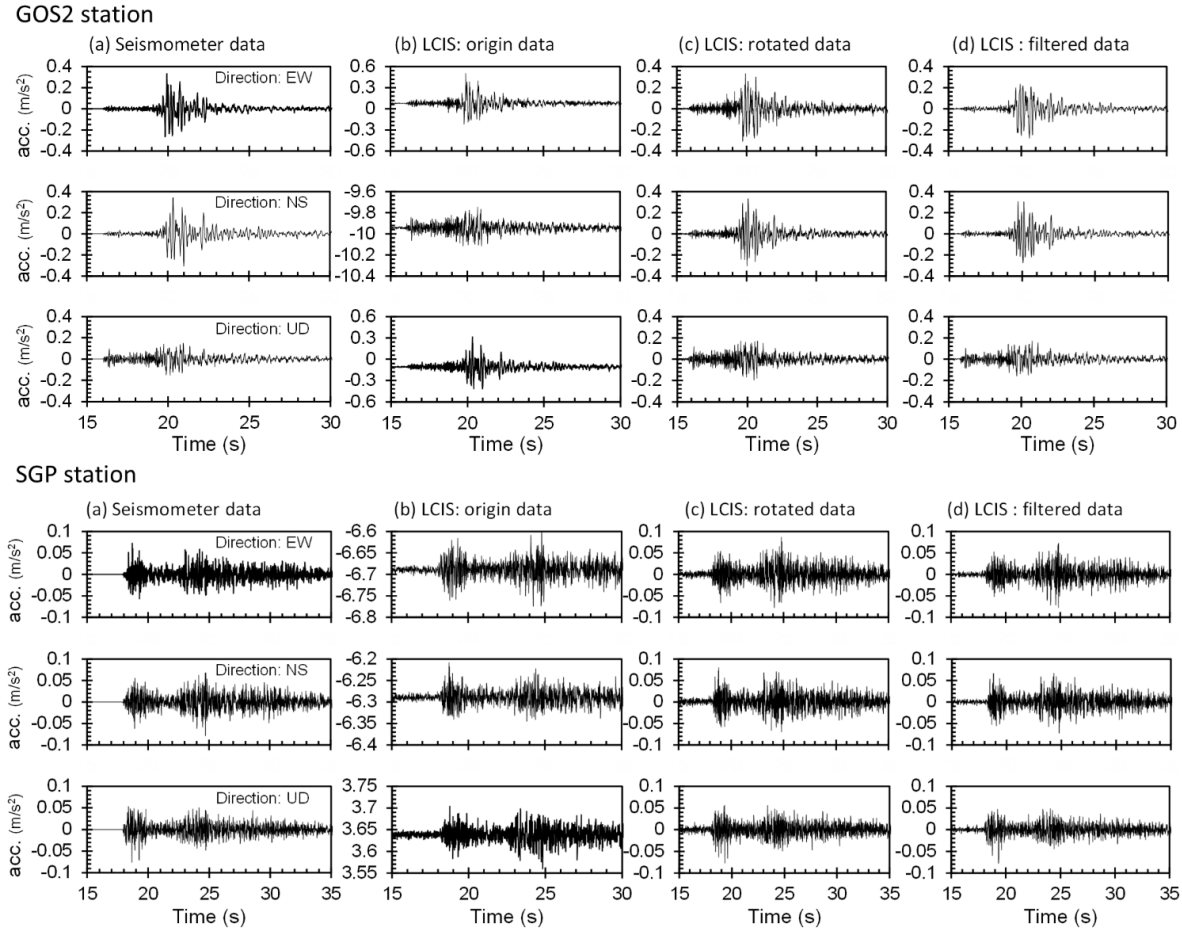

FIGURE 5. Comparison of high-performance seismometer of KMA and LCIS data at GOS2 (upper row) and SGP (lower row) observatories: (a) KMA seismometer record; (b) original LCIS data; (c) mapped LCIS data in east–west, north–south, and up–down directions; (d) filtered LCIS data.

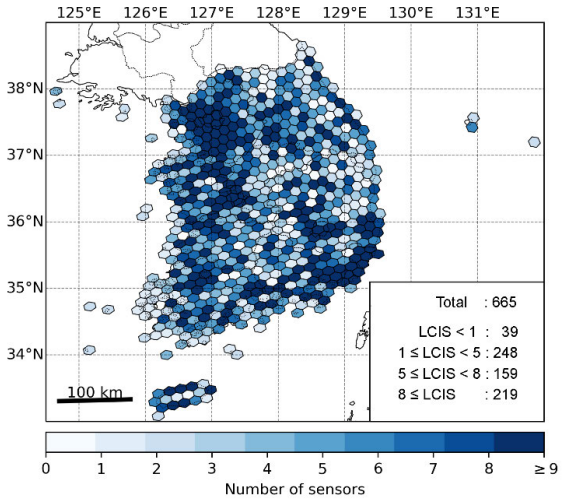

FIGURE 6. Number of LCIS devices in hexagonal grids.

components (north-south and east-west) and one vertical component using Eqs. 3-4. After rotation, the LCIS waveform for each direction became similar with the seismometer data (Fig. 5c). After that, we applied a bandpass filter to the waveform to remove background noise from the LCIS record. We did not consider the building response in this case because the LCIS was installed on the ground. As a result, the amplitude of the processed waveform did not differ from that recorded by the high-performance seismometer (Fig. 5d). The calculated PGAs are summarized in Table 3. The north-south direction (NS) horizontal PGA value recorded by the high-performance seismometer was 0.342 m/s^2, while the LCIS was 0.308 m/s^2 smaller than that of the seismometer. For the SGP case, the NS horizontal PGA from the high-performance seismometer was 0.079 m/s^2 and the LCIS was 0.072 m/s^2. In both cases, the difference was less than 10%. These case histories confirmed that the LCIS was useful for estimating seismic intensity, at least for PGA values greater than 0.08 m/s^2.

IV. SEISMIC INTENSITY MAP

Although nearly 7,000 LCIS devices have been deployed nationwide, they were not uniformly distributed because the deployment locations were restricted to cellular network stations, post offices, and fire stations. Hence, the number of LCIS devices is proportional to the population density.

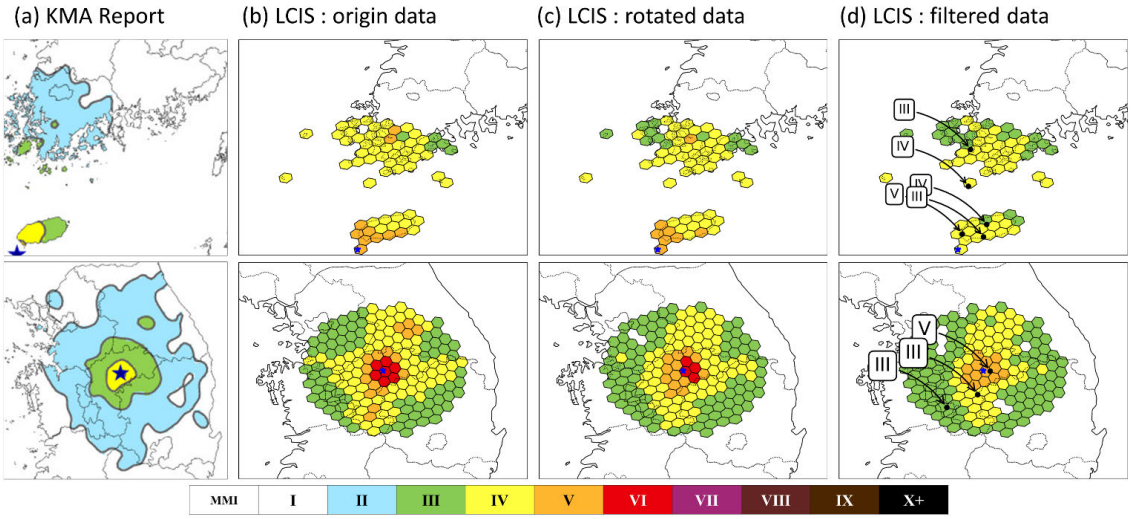

FIGURE 7. Comparison of seismic intensity maps between the KMA and LCIS networks. Upper row: M_L 4.9 coast of Seogwipo event. Lower row: M_L 4.1 Goesan event. (a) Map from official KMA report; (b) map from unprocessed LCIS data; (c) map from rotated LCIS data; (d) map from filtered LCIS data.

TABLE 3. Comparison of PGA at GOS2 and SGP observatories (unit:m/s^2).

Station	KMA seismometer		LCIS	
	Horizontal	Vertical	Horizontal	Vertical
GOS2	EW: 0.332	0.155	0.278	0.171
	NS: 0.342		0.308	
SGP	EW: 0.073	0.076	0.078	0.078
	NS: 0.079		0.072	

Considering this biased distribution of LCISs, we developed a method for generating an evenly weighted MMI map without ShakeMap [45], as explained next.

First, South Korea was divided into hexagonal grids. The length of the one side of the hexagon was set to 8.54 km to facilitate the division of administrative districts. Fig. 6 shows the number of sensors for each hexagon grid. Regions with six or more sensors in the grid are densely populated area. Some mountainous areas do not have any LCIS sensors. Second, we calculate the average PGA of LCISs in the hexagonal grid and convert to the MMI for the representative value. When an earthquake occurs, seismic waves were propagated at variable-sized amplitudes in a zone (i.e. grid) because of the site and path effects making it unreliable to rely solely on one seismic sensor to represent an entire area when determining MMI. Additionally, the accuracy of LCIS data is less sophisticated compared to high-performance seismometers, making it more dependent on the installation environment. Therefore, we are not recommended to rely on a single LCIS to provide a representative value of MMI at a hexagonal grid. Thus, we calculate only if the number of sensors was greater than two. We applied an interpolation algorithm based on MMI values from six connected grids for grids with less than three sensors. Note that earthquake signals detected using the Khan and Kwon [46] model are only counted for representative MMI calculation, and by user the representative value can be set as the median instead of the average.

Fig. 7 shows MMI distribution maps for two earthquakes in South Korea. Fig. 7a show the official KMA MMI map for the M_L 4.9 coast of Seogwipo earthquake that occurred in the Seogwipo area on December 14, 2021 (upper row) and the M_L 4.1 Goesan earthquake that occurred in the Goesan area on October 29, 2022 (lower row). Fig. 7d show the corresponding MMI maps generated from LCIS data. The KMA map is generated by first estimating IMs using a ground motion model (GMM) [47] and next interpolating observations from low-density network of high-performance seismometers. The LCIS maps use only LCIS data and interpolation, not GMM.

We found that if the LCIS data were used without rotation and filter, the MMIs would be overestimated (Fig. 7b). Moreover, the processed LCIS-based map shows an MMI value about 1 to 2 grades higher than the KMA map (Fig. 7a and 7d). The KMA map uses borehole seismometers, and the site amplification factor applying to the borehole records is often biased producing biased distribution [48]. Fig. 7d shows the MMI values from high-performance seismometers located at surface (black dots). We found that the seismic intensities from the LCIS map are closer to the observed MMI.

V. CONCLUSION

More than 7,000 stand-alone LCIS devices encompassing a MEMS accelerometer and an LTE communication sensor with real-time connectivity have been distributed across South Korea and are in operation as a seismic network. This network is 25 times denser than the existing national seismic network, and is expected to function as an intensity map generator with improved resolution and a faster EEW system. However, due to high background noise levels of LCISs and installation conditions, it is necessary to pre-process the LCIS

data to use for MMI map estimation. We propose three pre-processing steps to calculate the MMI and to reduce biased estimates.

First, we rotate the axes of the LCIS to have two horizontal and one vertical components. Second, we apply a band-pass filter to minimize high level background noise. Third, we remove the building response using a transfer function from the building floor to the ground surface, which is determined through MDOF analysis. Pre-processed LCIS data are comparable to those of high-performance seismometers based on case histories.

For MMI map generation, owing to the biased density of LCIS installations, we divided South Korea into hexagonal grids and used the average PGA for the representative MMI for each grid. If no LCISs were within one grid, the MMI for the grid was found by interpolating six encompassing grid values. We confirmed that this approach was effective for intensity map generation by validating it with MMI distributions from two earthquake events. The limitation was that I and II of MMI values could not be estimated because of the high background noise of LCIS.

Due to high density of LCIS devices, the MMI map can be generated without use of ground motion prediction models that depend on earthquake source, path, and site information, which includes prediction uncertainty. Direct use of observed LCIS records provides less uncertain seismic intensity estimation especially to high population area where the LCIS devices are densely distributed.

The results of this study confirm the suitability of MEMS-based IoT sensors as an alternative to conventional seismic observation networks. Information technology keeps evolving, so we expect that the advancement of sensors and networks will beneficially influence earthquake monitoring and warning systems.

ACKNOWLEDGMENT

The opinions, findings, and conclusions expressed in this material are those of the authors and do not necessarily reflect those of the KMA and Hanyang University. The authors declare that they have no known competing financial interests or personal relationships that could have appeared to influence the work reported in this paper.

REFERENCES

[1] S. E. Minson, A. S. Baltay, E. S. Cochran, T. C. Hanks, M. T. Page, S. K. McBride, K. R. Milner, and M.-A. Meier, "The limits of earthquake early warning accuracy and best alerting strategy," *Sci. Rep.*, vol. 9, no. 1, p. 2478, Feb. 2019, doi: 10.1038/s41598-019-39384-y.

[2] R. M. Allen and D. Melgar, "Earthquake early warning: Advances, scientific challenges, and societal needs," *Annu. Rev. Earth Planet. Sci.*, vol. 47, no. 1, pp. 361–388, 2019, doi: 10.1146/annurev-earth-053018-060457.

[3] H. Kanamori, "Real-time earthquake damage mitigation measures," in *Earthquake Early Warning Systems*. Berlin, Germany: Springer, 2007, pp. 1–8, doi: 10.1007/978-3-540-72241-0_1.

[4] M. Meier, Y. Kodera, M. Böse, A. Chung, M. Hoshiba, E. Cochran, S. Minson, E. Hauksson, and T. Heaton, "How often can earthquake early warning systems alert sites with high-intensity ground motion?" *J. Geophys. Res., Solid Earth*, vol. 125, no. 2, Feb. 2020, Art. no. e2019JB017718, doi: 10.1029/2019JB017718.

[5] C. Peng, P. Jiang, Q. Ma, J. Su, Y. Cai, and Y. Zheng, "Chinese nationwide earthquake early warning system and its performance in the 2022 Lushan M6.1 earthquake," *Remote Sens.*, vol. 14, no. 17, p. 4269, Aug. 2022, doi: 10.3390/rs14174269.

[6] S. Cho, J. K. Ahn, and E. H. Hwang, "Optimization of network-based earthquake early warning systems on the Korean Peninsula," *IEEE Access*, vol. 10, pp. 83931–83939, Aug. 2022, doi: 10.1109/ACCESS.2022.3197661.

[7] R. Bogue, "MEMS sensors: Past, present and future," *Sensor Rev.*, vol. 27, no. 1, pp. 7–13, Jan. 2007, doi: 10.1108/02602280710729068.

[8] A. S. Algamili, M. H. M. Khir, J. O. Dennis, A. Y. Ahmed, S. S. Alabsi, S. S. Ba Hashwan, and M. M. Junaid, "A review of actuation and sensing mechanisms in MEMS-based sensor devices," *Nanosc. Res. Lett.*, vol. 16, no. 1, pp. 1–21, Jan. 2021, doi: 10.1186/s11671-021-03481-7.

[9] A. Sabato, M. Q. Feng, Y. Fukuda, D. L. Carní, and G. Fortino, "A novel wireless accelerometer board for measuring low-frequency and low-amplitude structural vibration," *IEEE Sensors J.*, vol. 16, no. 9, pp. 2942–2949, May 2016, doi: 10.1109/JSEN.2016.2522940.

[10] J. K. Saunders, D. E. Goldberg, J. S. Haase, Y. Bock, D. G. Offield, D. Melgar, J. Restrepo, R. B. Fleischman, A. Nema, J. Geng, C. Walls, D. Mann, and G. S. Mattioli, "Seismogeodesy using GPS and low-cost MEMS accelerometers: Perspectives for earthquake early warning and rapid response," *Bull. Seismolog. Soc. Amer.*, vol. 106, no. 6, pp. 2469–2489, Dec. 2016, doi: 10.1785/0120160062.

[11] G. B. Tanircan, H. Alcik, and K. Beyen, "Reliability of MEMS accelerometers for instrumental intensity mapping of earthquakes," *Ann. Geophys.*, vol. 60, no. 6, p. 673, Jan. 2018, doi: 10.4401/ag-7501.

[12] M. Zhao and X. Xiong, "A new MEMS accelerometer applied in civil engineering and its calibration test," in *Proc. 9th Int. Conf. Electron. Meas. Instrum.*, Aug. 2009, pp. 2–122, doi: 10.1109/ICEMI.2009.5274629.

[13] I. Koene, R. Viitala, and P. Kuosmanen, "Internet of Things based monitoring of large rotor vibration with a microelectromechanical systems accelerometer," *IEEE Access*, vol. 7, pp. 92210–92219, 2019, doi: 10.1109/ACCESS.2019.2927793.

[14] S. Kim, I. Khan, S. Choi, and Y. W. Kwon, "Earthquake alert device using a low-cost accelerometer and its services," *IEEE Access*, vol. 9, pp. 121964–121974, Aug. 2021, doi: 10.1109/ACCESS.2021.3103505.

[15] R. Clayton, T. Heaton, M. Chandy, A. Krause, M. Kohler, J. Bunn, R. Guy, M. Olson, M. Faulkner, M. H. Cheng, L. Strand, R. Chandy, D. Obenshain, A. Liu, and M. Aivazis, "Community seismic network," *Ann. Geophys.*, vol. 54, no. 6, 738-747, 2011, doi: 10.3929/ethz-b-000044025.

[16] E. S. Cochran, J. F. Lawrence, C. Christensen, and R. S. Jakka, "The quake-catcher network: Citizen science expanding seismic horizons," *Seismolog. Res. Lett.*, vol. 80, no. 1, pp. 26–30, Jan. 2009, doi: 10.1785/gssrl.80.1.26.

[17] Q. Kong, R. M. Allen, L. Schreier, and Y.-W. Kwon, "MyShake: A smartphone seismic network for earthquake early warning and beyond," *Sci. Adv.*, vol. 2, no. 2, Feb. 2016, Art. no. e1501055, doi: 10.1126/sciadv.1501055.

[18] Y. M. Wu and T. L. Lin, "A test of earthquake early warning system using low cost accelerometer in Hualien, Taiwan," in *Early Warning for Geological Disasters*, F. Wenzel and J. Zschau, Eds. Berlin, Germany: Springer, 2014, pp. 253–261, doi: 10.1007/978-3-642-12233-0_13.

[19] Y. M. Wu and H. Mittal, "A review on the development of earthquake warning system using low-cost sensors in Taiwan," *Sensors*, vol. 2, no. 22, p. 7649, Nov. 2021, doi: 10.3390/s21227649.

[20] Y. M. Wu, "Progress on development of an earthquake early warning system using low-cost sensors," *Pure Appl. Geophys.*, vol. 172, no. 9, pp. 2343–2351, Sep. 2015, doi: 10.1007/s00024-014-0933-5.

[21] C. Peng, X. Zhu, J. Yang, B. Xue, and Y. Chen, "Development of an integrated onsite earthquake early warning system and test deployment in Zhaotong, China," *Comput. Geosci.*, vol. 56, pp. 170–177, Jul. 2013, doi: 10.1016/j.cageo.2013.03.018.

[22] C. Peng, Y. Chen, Q. Chen, J. Yang, H. Wang, X. Zhu, Z. Xu, and Y. Zheng, "A new type of tri-axial accelerometers with high dynamic range MEMS for earthquake early warning," *Comput. Geosci.*, vol. 100, pp. 179–187, Mar. 2017, doi: 10.1016/j.cageo.2017.01.001.

[23] Y. W. Kwon, J. K. Ahn, J. Lee, and C. H. Lee, "Earthquake early warning using low-cost MEMS sensors," in *Proc. IEEE Int. Geosci. Remote Sens. Symp.*, Sep. 2020, pp. 6635–6637, doi: 10.1109/IGARSS39084.2020.9323438.

[24] A. Wu, J. Lee, I. Khan, and Y. W. Kwon, "CrowdQuake+: Data-driven earthquake early warning via IoT and deep learning," in *Proc. IEEE Int. Conf. Big Data (Big Data)*, Dec. 2021, pp. 2068–2075, doi: 10.1109/BigData52589.2021.9671971.

[25] D. J. Wald, C. B. Worden, E. M. Thompson, and M. Hearne, "ShakeMap operations, policies, and procedures," *Earthq. Spectra*, vol. 38, no. 1, pp. 756–777, Feb. 2022, doi: 10.1177/87552930211030298.
[26] B. M. Yang, H. Mittal, and Y.-M. Wu, "Real-time production of PGA, PGV, Intensity, and Sa shakemaps using dense MEMS-based sensors in Taiwan," *Sensors*, vol. 21, no. 3, p. 943, Jan. 2021, doi: 10.3390/s21030943.
[27] D. Jang, J. K. Ahn, Y. Kwon, and D. Kwak, "Comparative analysis of seismic records observed at seismic stations and smartphone MEMS sensors," *KSCE J. Civil Environ. Eng. Res.*, vol. 41, no. 5, pp. 513–522, 2021, doi: 10.12652/Ksce.2021.41.5.0513.
[28] Korea Meteorological Administration (KMA), "Performance and standards for seismic equipment," (in Kroean), Korea Meteorological Administration Notification 2018-11, Enforced 31, Dec. 2018.
[29] J. F. Clinton and T. H. Heaton, "Potential advantages of a strong-motion velocity meter over a strong-motion accelerometer," *Seismolog. Res. Lett.*, vol. 73, no. 3, pp. 332–342, May 2002, doi: 10.1785/gssrl.73.3.332.
[30] J. Peterson, "Observations and modeling of background seismic noise," U.S. Geol. Surv., Albuquerque, NM, USA, Open-File Rep. 93-322, 1993, doi: 10.3133/ofr93322.
[31] C. Cauzzi and J. Clinton, "A high- and low-noise model for high-quality strong-motion accelerometer stations," *Earthq. Spectra*, vol. 29, no. 1, pp. 85–102, Feb. 2013, doi: 10.1193/1.4000107.
[32] W. Lee, T. S. Song, and J.-H. Youn, "Detection of fall direction using a velocity vector in the Android smartphone environment," *J. Korea Inst. Inf. Commun. Eng.*, vol. 19, no. 2, pp. 336–342, Feb. 2015, doi: 10.6109/jkiice.2015.19.2.336.
[33] S. Abbate, M. Avvenuti, F. Bonatesta, G. Cola, P. Corsini, and A. Vecchio, "A smartphone-based fall detection system," *Pervasive Mobile Comput.*, vol. 8, no. 6, pp. 883–899, Dec. 2012, doi: 10.1016/j.pmcj.2012.08.003.
[34] S. Thiemjarus, "A device-orientation independent method for activity recognition," in *Proc. Int. Conf. Body Sensor Netw.*, Jun. 2010, pp. 19–23, doi: 10.1109/BSN.2010.55.
[35] I. Choi, J. K. Ahn, and D. Kwak, "A fundamental study on the database of response history for historical earthquake records on the Korean Peninsula," (in Korean), *KSCE J. Civil Environ. Eng. Res.*, vol. 39, no. 6, pp. 821–831, Dec. 2019, doi: 10.12652/Ksce.2019.39.6.0821.
[36] J. K. Ahn, D. Y. Kwak, I. H. Choi, J. Lee, and D. Lim, "Method for providing seismic time series data analysis, recording medium and device for performing the method," (in Korean), Korean Patent Appl.10-2021-0 063 471, Mar. 22, 2022.
[37] N. Bastías and G. A. Montalva, "Chile strong ground motion flatfile," *Earthq. Spectra*, vol. 32, no. 4, pp. 2549–2566, Nov. 2016, doi: 10.1193/102715EQS158DP.
[38] H. M. Dawood, A. Rodriguez-Marek, J. Bayless, C. Goulet, and E. Thompson, "A flatfile for the KiK-Net database processed using an automated protocol," *Earthq. Spectra*, vol. 32, no. 2, pp. 1281–1302, May 2016, doi: 10.1193/071214eqs106.
[39] G. Lanzano, S. Sgobba, L. Luzi, R. Puglia, F. Pacor, C. Felicetta, M. D'Amico, F. Cotton, and D. Bindi, "The pan-European engineering strong motion (ESM) flatfile: Compilation criteria and data statistics," *Bull. Earthq. Eng.*, vol. 17, no. 2, pp. 561–582, Feb. 2019, doi: 10.1007/s10518-018-0480-z.
[40] J. A. Schultz and C. H. Raebel, "Harvesting of ambient floor vibration energy utilizing micro-electrical mechanical devices," in *Special Topics in Structural Dynamics*, R. Allemang, J. De Clerck, C. Niezrecki, and A. Wicks, Eds. New York, NY, USA: Springer, 2013, pp. 561–570, doi: 10.1007/978-1-4614-6546-1_59.
[41] J. Lee, J. H. Sim, J. K. Ahn, and Y. W. Kwon, "An open dataset for deep learning-based earthquake detection using MEMS sensors," in *Proc. IEEE Int. Conf. Big Data (Big Data)*, Dec. 2022, pp. 6755–6757, doi: 10.1109/bigdata55660.2022.10020481.
[42] Incorporated Research Institution for Seismology (IRIS), "SEED reference manual-standard for the exchange of earthquake data, seed format version 2.4," Int. Fed. Digit. Seismograph Netw., United States Geol. Surv., Aug. 2012, p. 217.
[43] A. T. Ringler, M. T. Hagerty, J. Holland, A. Gonzales, L. S. Gee, J. D. Edwards, D. Wilson, and A. M. Baker, "The data quality analyzer: A quality control program for seismic data," *Comput. Geosci.*, vol. 76, pp. 96–111, Mar. 2015, doi: 10.1016/j.cageo.2014.12.006.
[44] D. Robinson, T. Dhu, and J. Schneider, "SUA: A computer program to compute regolith site-response and estimate uncertainty for probabilistic seismic hazard analyses," *Comput. Geosci.*, vol. 32, no. 1, pp. 109–123, Feb. 2006, doi: 10.1016/j.cageo.2005.02.017.
[45] S. A. Verros, D. J. Wald, C. B. Worden, M. Hearne, and M. Ganesh, "Computing spatial correlation of ground motion intensities for ShakeMap," *Comput. Geosci.*, vol. 99, pp. 145–154, Feb. 2017, doi: 10.1016/j.cageo.2016.11.004.
[46] I. Khan and Y. W. Kwon, "P-detector: Real-time P-wave detection in a seismic waveform recorded on a low-cost MEMS accelerometer using deep learning," *IEEE Geosci. Remote Sens. Lett.*, vol. 19, pp. 1–5, Mar. 2022, doi: 10.1109/LGRS.2022.3161017.
[47] A. Emolo, N. Sharma, G. Festa, A. Zollo, V. Convertito, J. Park, H. Chi, and I. Lim, "Ground-motion prediction equations for South Korea Peninsula," *Bull. Seismolog. Soc. Amer.*, vol. 105, no. 5, pp. 2625–2640, Oct. 2015, doi: 10.1785/0120140296.
[48] D. Lim and J. K. Ahn, "Horizontal seismic wave at ground surface from transfer function based on ambient noise," *Frontiers Earth Sci.*, vol. 11, Mar. 2023, doi: 10.3389/feart.2023.1047667.

JAE-KWANG AHN received the B.S., M.S., and Ph.D. degrees from Hanyang University, South Korea, in 2006, 2008, and 2017, respectively, and the M.P.A. degree from Chung-Ang University, South Korea, in 2021. He is currently a Research Officer with Korea Meteorological Administration. His research interests include social science, earthquake, ground motion, EEW, seismic engineering, liquefaction, the IoT sensor, GANs, and data science.

JANGSOO LEE received the B.S. and M.S. degrees from Kyungpook National University, in 2018 and 2020, respectively, where he is currently pursuing the Ph.D. degree with the School of Computer Science and Engineering. His research interests include the IoT, middleware, and distributed systems.

YOUNG-WOO KWON (Member, IEEE) received the Ph.D. degree in computer science from Virginia Tech, in 2014. He is currently an Associate Professor with the School of Computer Science and Engineering, Kyungpook National University. Before coming to Kyungpook National University, he was an Assistant Professor with the Department of Computer Science, Utah State University. His research interests include distributed systems, the IoT, and disaster management.

JUNG-KYU KIM received the B.S. degree in electrotechnology from Kyungpook National University, in 2011. He is currently the Manager with SK Telecom, a key telecommunication operator in South Korea. His research interest includes social enterprise activities to create a safe society from earthquake disasters.

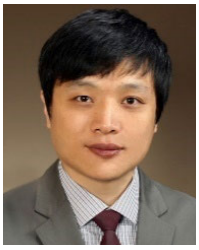

DONG YOUP KWAK received the Ph.D. degree in civil and environmental engineering from the University of California at Los Angeles, in 2014. He is currently an Associate Professor with the Department of Civil and Environmental Engineering, Hanyang University, ERICA Campus. Before coming to Hanyang University, he was a Senior Modeler with Risk Management Solutions Inc. His research interests include ground motion modeling, site amplification, site characterization, and seismic hazard analysis.